FREE CONVECTION OF A NANOFLUID IN A SQUARE CAVITY WITH A HEAT SOURCE ON THE BOTTOM WALL AND PARTIALLY COOLED FROM SIDES

by

Mostafa MAHMOODI[a*], Ali Akbar ABBASIAN ARANI[b], Saeed MAZROUEI SEBDANI[b], Saeed NAZARI[b], and Mohammad AKBARI[c]

[a] Department of Mechanical Engineering, Najafabad Branch, Islamic Azad University, Isfahan, Iran
[b] Mechanical Engineering Department, Amirkabir University of Technology, Tehran, Iran

Original scientific paper
DOI: 10.2298/TSCI110406011A

The problem of free convection fluid flow and heat transfer in a square cavity with a flush mounted heat source on its bottom wall and two heat sinks on its vertical side walls has been investigated numerically. Via changing the location of the heat sinks, six different arrangements have been generated. The cavity was filled with Cu-water nanofluid. The governing equations were discretized using the finite volume method and SIMPLER algorithm. Using the developed code, a parametric study was undertaken, and effects of Rayleigh number, arrangements of the heat sinks and volume fraction of the nanoparticles on fluid flow and heat transfer inside the cavity were investigated. Also for the middle-middle heat sinks arrangement, capability of five different water based nanofluids on enhancement of the rate of heat transfer was examined and compared. From the obtained results it was found that the average Nusselt number, for all six different arrangements of the heat sinks, was an increasing function of the Rayleigh number and the volume fraction of the nanoparticles. Also it was found that at high Rayleigh numbers, maximum and minimum average Nusselt number occurred for middle-middle and top-bottom arrangement, respectively. Moreover it was found that for the middle-middle arrangement, at high Rayleigh numbers, maximum and minimum rate of heat transfer was obtained by Cu-water and TiO_2-water nanofluids, respectively.

Key words: *free convection, numerical simulation, square cavity, nanofluid, heat sinks*

Introduction

Free convection fluid flow and heat transfer is an important phenomenon which occurs in many industrial and engineering processes such as electronic equipment cooling, ventilation, heating and cooling of rooms, insolation of reactors, solar collector, *etc*. [1]. In these systems low thermal conductivity of traditional used coolant such as oil, water, and ethylene glycol, is an important limitation to obtaining maximum thermal efficiency. A nanofluid, which is a suspension of nano-sized solid particles in a base fluid, has higher thermal conductivity than the based fluid, hence can be used to increase the rate of heat transfer in different applications [2]. Different aspects of nanofluids have been studied by many researchers such as works of Kang *et al.* [3] about thermal conductivity of nanofluids, Velagapudi *et al.* [4] about thermophysical properties of nanofluids, Turgut *et al.* [5] about viscosity of nanofluids,

* Corresponding author; e-mail: mmahmoodi46@gmail.com

Rudyak *et al.* [6] and Murugesan and Sivan [7] about thermal conductivity of nanofluids, and Nayak *et al.* [8] about thermal expansion coefficient of nanofluids.

First work on numerical study of free convection fluid flow and heat transfer of nanofluids inside rectangular cavities was done by Khanafer *et al.* [9]. They observed that the rate of heat transfer increases when the volume fraction of the nanoparticles increases for the entire range of Grashof number considered. Non-Newtonian behavior of Cu-water nanofluid on free convection heat transfer inside rectangular cavities was studied by Santra *et al.* [10] numerically. They found that rate of heat transfer decreases with increase of the volume fraction of the nanoparticles for a particular Rayleigh number, while it increases with Rayleigh number for a particular volume fraction of the nanoparticles. Numerical study of free convection heat transfer inside partially heated rectangular cavities filled with different water based nanofluids was done by Oztop and Abu-Nada [11]. The cavities had a cold vertical wall, a localized heater on the other vertical wall and insulated horizontal walls. In their study effects of Rayleigh number, aspect ratio of cavities, size and location of the heater, and different types of water based nanofluids were investigated. The obtained results showed that the average Nusselt number of the heat source increased with increase of the volume fraction of the nanoparticles and height of heater for all range of Rayleigh numbers considered. In another numerical study, Abu-Nada and Oztop [12] investigated effect of inclination angle of a square cavity filled with Cu-water on free convection fluid flow and heat transfer inside it. In their study it was observed that effects of inclination angle on percentage of heat transfer enhancement became insignificant at low Rayleigh number. Using a numerical study, Aminossadati and Ghasemi [13] investigated free convection inside a nanofluid filled square cavity with cold vertical and top horizontal walls and a constant heat flux heater on its horizontal bottom wall. Effects of Rayleigh number, volume fraction of the nanoparticles, size and location of heater and type of nanofluid on heat transfer and fluid flow were considered in their study. They found that nanoparticles improve the rate of heat transfer especially at low Rayleigh numbers. Also it was found that type of nanoparticles and the length and location of the heat source affected significantly the heat source maximum temperature. Numerical investigation of periodic free convection fluid flow and heat transfer inside a nanofluid filled square cavity has been done by Ghasemi and Aminossadati [14]. They considered a square cavity with insulated top and bottom walls, cold right vertical wall and a heater with oscillating heat flux on its left vertical wall. They observed a periodic behavior of flow and temperature fields as a result of the oscillating heat flux. Moreover it was found that optimum position of the heat source on the left wall is a function of Rayleigh number. Saleh *et al.* [15] investigated numerically free convection of nanofluid in a trapezoidal enclosure and developed a correlation for the average Nusselt number as a function of the angle of the sloping wall, effective thermal conductivity and viscosity as well as Grashof number. Sheikhzadeh *et al.* [16] conducted a numerical simulation to investigate problem of free convection of the TiO_2-water nanofluid in rectangular cavities differentially heated on adjacent walls. The left and the top walls of the cavities were heated and cooled, respectively, while the cavities right and bottom walls were kept insulated. They found that by increase in volume fraction of the nanoparticles, mean Nusselt number of the hot wall increased for the shallow cavities, while the reverse trend occurred for the tall cavities. Very recently numerical results of a study on free convection in a nanofluid filled square cavity by using heating and cooling by sinusoidal temperature profiles on one side were reported by Oztop *et al.* [17]. They considered effects of various inclination angles of the cavity, different types of water based nanofluids, volume fraction of nanoparticles, and

Rayleigh number on heat transfer rate. They found that addition of nanoparticle into the water affected the fluid flow and temperature distribution especially for higher Rayleigh numbers. Free convection of nanofluids in square cavities with an inside thin heater were investigated by Abbasian Arani *et al.* [18] and Mahmoodi [19]. Results of numerical studies on free convection in nanofluid filled L-shaped cavities were reported by Mahmoodi [20] and Sourtiji and Hosseinizadeh [21].

Free convection inside square cavities with discrete flush-mounted heat sources and sinks has complex nature and hence has received considerable attention because of its importance and wide applications in buildings or cooling of flush mounted electronic heaters in modern electronic devices and supercomputers. Nithyadevi *et al.* [22] conducted a numerical study to investigate effect of aspect ratio on the free convection in a rectangular cavity with partially thermally active side walls. The obtained results showed that the heat transfer rate increases when the aspect ratio increases. Laminar free convection in a 2-D square cavity due to two and three pairs of discrete heat source and sink on vertical side walls was investigated numerically by Deng [23]. The sizes of sources and sinks were 1/4 and 1/6 of the height of the cavity for two and three pairs of sources and sinks, respectively. It was found that the total heat transfer was closely related with the number of eddies in the enclosure and when the sources and sinks were split into smaller segments, the number of eddies in the enclosure would increase and hence the heat transfer was augmented. Sheikhzadeh *et al.* [24] conducted a numerical simulation to study free convection of Cu-water nanofluid inside a square cavity with partially thermally active side walls. The active parts of the left and the right side walls of the cavity were maintained hot and cold, respectively, while the cavity's top and bottom walls as well as the inactive parts of the side walls were kept insulated. They observed that average Nusselt number increased when both Rayleigh number and volume fraction of nanoparticles increased. Moreover they found that maximum average Nusselt number at high Rayleigh numbers occurred when the hot and cold parts were located on the bottom and middle region of the vertical walls, respectively.

In the present paper, the problem of free convection in a square cavity heated from below and partially cooled from the side walls filled with the Cu-water nanofluid is studied numerically. Six different cases, according to the location of discrete heat sinks on the vertical walls of the cavity, are considered. When the heat sinks are located on the vertical walls in different positions, different flow patterns can be formed *via* interaction between buoyancy effects of the heat sinks, hence for each position of the heat sinks different cooling performance (rate of heat transfer) is obtained. Therefore investigation of natural convection fluid flow and heat transfer for different position of the heat sinks on the vertical walls leads to obtaining best position of the heat sinks for maximum rate of heat transfer. The finite volume method with SIMPLER algorithm is used to discretize non-linear coupled partial differential equations of flow and pressure fields. The effects of locations of heat sinks on the vertical walls, the volume fraction of the nanoparticles, and Rayleigh number on fluid flow and heat transfer inside the enclosure are investigated. Moreover for middle-middle arrangements of the heat sinks, capability of five different water based nanofluids on enhancement of the heat transfer is examined.

Mathematical modeling

A schematic view of the square cavity with six different arrangements of heat sinks on its side walls considered in the present study is shown in fig. 1. The height and the width of the cavity are denoted by H and W, respectively, that for square cavity $H = W$. A heat

source with the length of $H/2$ is located in the middle of the bottom wall. The length of the two heat sinks is $H/2$ that by change of relative locations of the heat sinks along the vertical walls of the cavity six different arrangements are generated as shown in fig. 1. The heat source is kept at hot temperature T_h, while the heat sinks are kept at cold temperature T_c. The horizontal top wall and the inactive portion of the vertical and horizontal bottom walls of the cavity are kept insulated. The length of the cavity perpendicular to its plane is assumed to be long enough; hence, the problem is considered two dimensional. The cavity is filled with Cu-water nanofluid. It is assumed that the nanoparticles and the base fluid are in thermal equilibrium and there is no slip between them. The thermophysical properties of nanoparticles and the water as the base fluid at $T = 25°$ are listed in tab. 1. The nanofluid is considered Newtonian, laminar, and incompressible. The thermophysical properties of the nanofluid are considered constant with the exception of the density which varies according to the Boussinesq approximation [25].

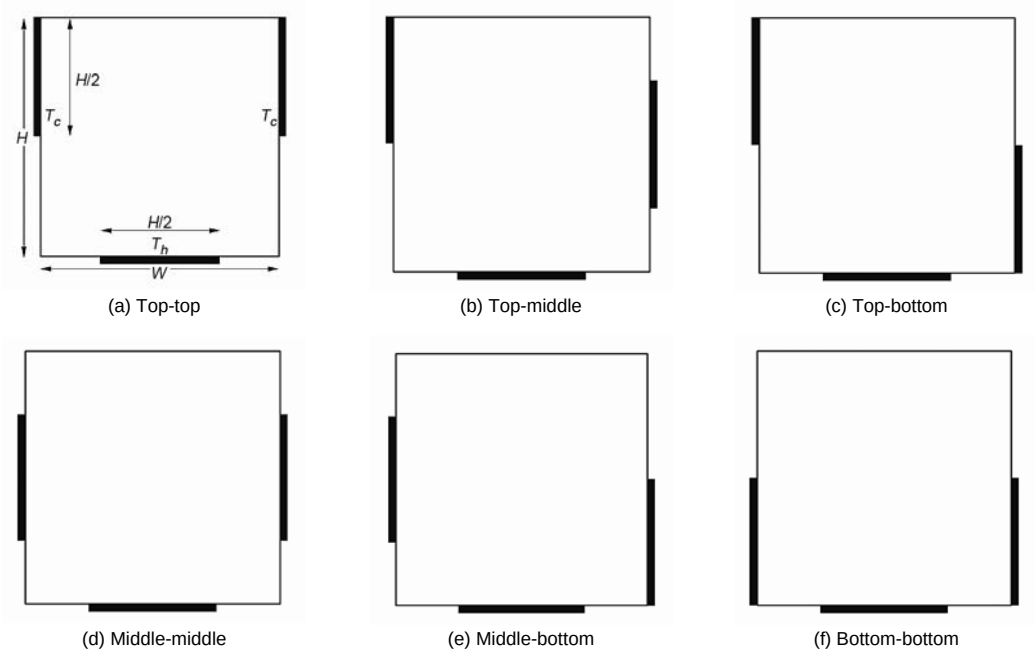

(a) Top-top (b) Top-middle (c) Top-bottom

(d) Middle-middle (e) Middle-bottom (f) Bottom-bottom

Figure 1. Schematic view of the square cavity with six different arrangements of the heat sinks

Table 1. Thermophysical properties of the base fluid and nanoparticles at $T = 25$ K

Thermophysical properties	Water	Cu	Ag	Al_2O_3	CuO	TiO_2
C_p [$Jkg^{-1}K^{-1}$]	4179	385	235	765	535.6	686.2
ρ [kgm^{-3}]	997.1	8933	10500	3970	6500	4250
k [$Wm^{-1}K^{-1}$]	0.613	400	429	40	20	8.95
$\beta \cdot 10^{-5}$ [K^{-1}]	21	1.67	1.89	0.85	1.67	0.9

The continuity, momentum and energy equations for 2-D laminar free convection fluid flow and heat transfer with the Boussinesq approximation in y-direction are:

$$\frac{\partial u}{\partial x}+\frac{\partial v}{\partial y}=0 \tag{1}$$

$$u\frac{\partial u}{\partial x}+v\frac{\partial u}{\partial y}=-\frac{1}{\rho_{nf}}\frac{\partial p}{\partial x}+\frac{\mu_{nf}}{\rho_{nf}}\left(\frac{\partial^2 u}{\partial x^2}+\frac{\partial^2 u}{\partial y^2}\right) \tag{2}$$

$$u\frac{\partial v}{\partial x}+v\frac{\partial v}{\partial y}=-\frac{1}{\rho_{nf}}\frac{\partial p}{\partial y}+\frac{\mu_{nf}}{\rho_{nf}}\left(\frac{\partial^2 v}{\partial x^2}+\frac{\partial^2 v}{\partial y^2}\right)+\frac{(\rho\beta)_{nf}}{\rho_{nf}}\mathrm{g}(T-T_c) \tag{3}$$

$$u\frac{\partial T}{\partial x}+v\frac{\partial T}{\partial y}=\alpha_{nf}\left(\frac{\partial^2 T}{\partial x^2}+\frac{\partial^2 T}{\partial y^2}\right) \tag{4}$$

where the density, heat capacity, thermal expansion coefficient, and thermal diffusivity of the nanofluid are, respectively [9]:

$$\rho_{nf}=(1-\varphi)\rho_f+\varphi\rho_s \tag{5}$$

$$(\rho C_p)_{nf}=(1-\varphi)(\rho C_p)_f+\varphi(\rho C_p)_s \tag{6}$$

$$(\rho\beta)_{nf}=(1-\varphi)(\rho\beta)_f+\varphi(\rho\beta)_s \tag{7}$$

$$\alpha_{nf}=\frac{k_{nf}}{(\rho C_p)_{nf}} \tag{8}$$

The Brinkman model [26] is employed to estimate the effective dynamic viscosity of the nanofluid:

$$\mu_{eff}=\frac{\mu_f}{(1-\varphi)^{2.5}} \tag{9}$$

The effective thermal conductivity of the nanofluid with spherical nanoparticles is estimated according to Maxwell [27]:

$$\frac{k_{nf}}{k_f}=\frac{k_s+2k_f-2\varphi(k_f-k_s)}{k_f+2k_s+\varphi(k_f-k_s)} \tag{10}$$

These relations have been used in recently published works about numerical simulation of free convection of nanofluid [9, 11-15, 17].

The following dimensionless parameters are defined to convert the governing equation in dimensionless form:

$$X=\frac{x}{H},\quad Y=\frac{y}{H},\quad U=\frac{uH}{\alpha_f},\quad V=\frac{vH}{\alpha_f},\quad P=\frac{pH^2}{\rho_{nf}\,\alpha_f^2},\quad \theta=\frac{T-T_c}{T_h-T_c} \tag{11}$$

Using the dimensionless parameters, the non-dimensional forms of the governing equations are:

$$\frac{\partial U}{\partial X}+\frac{\partial V}{\partial Y}=0 \tag{12}$$

$$U\frac{\partial U}{\partial X}+V\frac{\partial U}{\partial Y}=-\frac{\partial P}{\partial X}+\frac{\mu_{nf}}{\rho_{nf}\alpha_f}\left(\frac{\partial^2 U}{\partial X^2}+\frac{\partial^2 U}{\partial Y^2}\right) \tag{13}$$

$$U\frac{\partial V}{\partial X}+V\frac{\partial V}{\partial Y}=-\frac{\partial P}{\partial Y}+\frac{\mu_{nf}}{\rho_{nf}\alpha_f}\left(\frac{\partial^2 V}{\partial X^2}+\frac{\partial^2 V}{\partial Y^2}\right)+\frac{(\rho\beta)_{nf}}{\rho_{nf}\beta_f}\mathrm{Ra}\,\mathrm{Pr}\,\theta \tag{14}$$

$$U\frac{\partial \theta}{\partial X}+V\frac{\partial \theta}{\partial Y}=\frac{\alpha_{nf}}{\alpha_f}\left(\frac{\partial^2 \theta}{\partial X^2}+\frac{\partial^2 \theta}{\partial Y^2}\right) \tag{15}$$

where the Rayleigh number (Ra), and the Prandtl number (Pr) are:

$$\mathrm{Ra}=\frac{\mathrm{g}\beta_f (T_h-T_c)H^3}{\alpha_f \nu_f},\quad \mathrm{Pr}=\frac{\nu_f}{\alpha_f} \tag{16}$$

The boundary conditions for eqs. 12-15 are:

$$\begin{aligned}&-\text{ on the heat source: } U=V=0,\quad \theta=1\\ &-\text{ on the heat sinks: } U=V=0,\quad \theta=0\\ &-\text{ on the insulated parts of the walls: } U=V=0,\quad \partial\theta/\partial n=0\end{aligned} \tag{17}$$

where n is normal direction to the walls.

The local Nusselt number of the heat source is expressed as:

$$\mathrm{Nu}_{\mathrm{local}}=\frac{hH}{k_f} \tag{18}$$

where the heat transfer coefficient is:

$$h=\frac{q_w}{T_h-T_c} \tag{19}$$

The thermal conductivity is calculated as:

$$k_{nf}=-\frac{q_w}{\partial T/\partial Y\big|_{Y=0}} \tag{20}$$

By substituting eqs. (20) and (19) in eq. (18), the Nusselt number can be written:

$$\mathrm{Nu}_{\mathrm{local}}=-\left(\frac{k_{nf}}{k_f}\right)\frac{\partial\theta}{\partial Y}\bigg|_{Y=0} \tag{21}$$

The average Nusselt number of the heat source is obtained by integrating the local Nusselt number along the heat source:

$$\mathrm{Nu}=2\int_{0.25}^{0.75}\mathrm{Nu}_{\mathrm{local}}\,\mathrm{d}X\bigg|_{Y=0} \tag{22}$$

Numerical approach

The dimensionless governing equations associated with the boundary conditions are solved numerically using the finite volume method. The hybrid-scheme, which is a combination of the central difference scheme and the upwind scheme, is used to discretize the convection terms while the second order central difference scheme is used to discretize the diffusion terms. A staggered grid system, in which the velocity components are stored midway between the scalar storage locations, is employed. In order to couple the velocity field and pressure in the momentum equations, the well-known SIMPLER algorithm is adopted [28]. The solution of the fully coupled discretized equations was obtained iteratively using the TDMA method [29]. The convergence criterion is defined by the expression:

$$Error = \frac{\sum_{j=1}^{m}\sum_{i=1}^{n}\left|\xi^{t+1}-\xi^{t}\right|}{\sum_{j=1}^{m}\sum_{i=1}^{n}\left|\xi^{t+1}\right|} \le 10^{-6} \tag{23}$$

where m and n are the number of grid points in x- and y- direction, respectively, ξ is a transport quantity, and t is the number of iteration.

In order to validate the obtained numerical code, two different test cases are employed using the presented code, and the results are compared with the existing results in the literature. The first test case is the problem of free convection in partially heated cavity filled with Cu-water nanofluid with φ = 0.1 shown in fig. 2(a). The second test case is free convection fluid flow and heat transfer in a differentially heated square cavity filled with air shown in fig. 2(b). Tables 2 and 3, show comparison between the average Nusselt numbers obtained by the present numerical simulation and those presented by other investigators for two considered test cases. As it can be observed from theses tables, very good agreements exist between the results of the current simulation with those of other investigators for two different test cases.

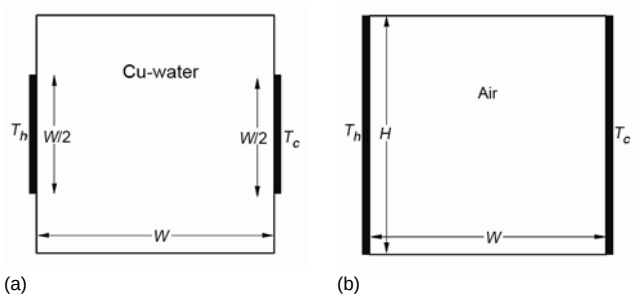

Figure 2. Domain and boundary conditions for the first (a) and second (b) used test case

Table 2. The average Nusselt number of the hot portion walls for the first test case, comparisons of the present results with the results of Sheikhzadeh *et al.* [24]

	Present study	Sheikhzadeh *et al.* [24]	Differences
Ra = 10^3	2.218	2.228	0.45%
Ra = 10^4	3.715	3.709	0.16%
Ra = 10^5	7.221	7.160	0.84%
Ra = 10^6	12.905	12.881	0.19%

In order to determine a proper grid for the numerical simulation, a grid independence study is undertaken for free convection inside the cavity filled with the Cu-water nanofluid with φ = 0.15, with middle-middle arrangement of the heat sinks while the Rayleigh number is kept at 10^6. Four different uniform grids, namely, 20 × 20, 40 × 40, 80 × 80, and 160 × 160 are employed and for each grid size,

Table 3. The average Nusselt number of the hot wall for the second test case, comparisons of the present results with the results of other investigators

	Ra = 10^3	Ra = 10^4	Ra = 10^5	Ra = 10^6
Present study	1.113	2.254	4.507	8.802
Barakos and Mitsoulis [30]	1.114	2.245	4.510	8.806
Davis [31]	1.118	2.243	4.519	8.799
Fusegi *et al.* [32]	1.105	2.302	4.646	9.012

dimensionless temperature and dimensionless vertical component of the velocity along the horizontal centerline of the cavity are obtained. Figure 3 shows the dimensionless vertical component of the velocity and dimensionless temperature along the horizontal centerline of the cavity for different grids obtained by the current simulation for Ra = 10^6. As it can be observed from the figure, an 80 × 80 uniform grid is sufficiently fine to ensure a grid independent solution. Based on these results, an 80 × 80 uniform grid is used for all the results to be presented in the paper.

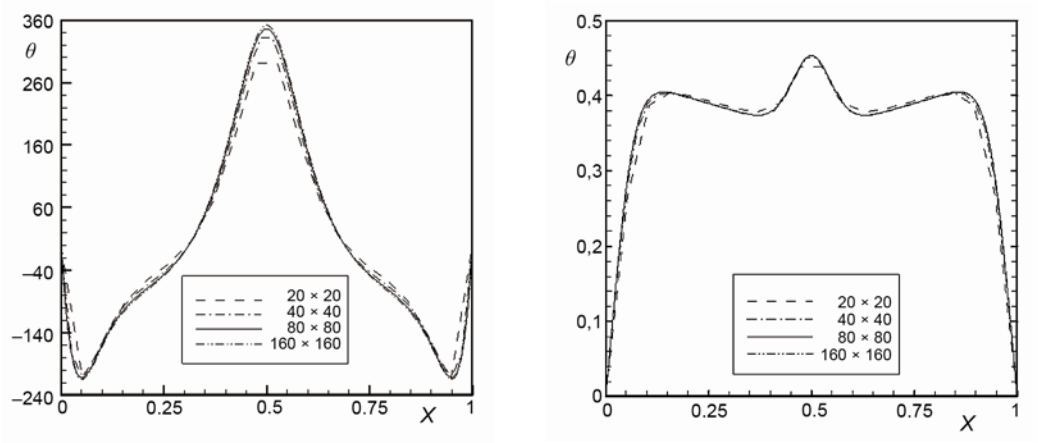

(a) (b)

Figure 3. Effect of the grid density on the dimensionless vertical component of velocity (a) and dimensionless temperature (b) along the horizontal centerline of the cavity for the middle-middle arrangement at Ra = 10^6 and φ = 0.15

Results and discussion

In this section, numerical results of free convection fluid flow and heat transfer of Cu-water nanofluid inside a square cavity partially heated from below and with two heat sinks on its vertical walls are presented. The results have been obtained for six different arrangements of heat sinks, namely, top-top, top-middle, top-bottom, middle-middle, middle-bottom, and bottom-bottom. For all considered arrangements of heat sinks, the length of the heat source and sinks is kept at 0.5, while the Rayleigh number is ranging from 10^3 to 10^6 and the volume fraction of the nanoparticles is varying from 0 to 0.15. Also for the middle-middle case, five different water based nanofluids, Cu-water, Ag-water, Al_2O_3-water, CuO-water, and TiO_2-water, are employed and their efficiency in enhancement of the rate of heat transfer is compared.

Streamlines and isotherms for nanofluid with φ = 0.15 and pure water for different arrangements of heat sinks at Ra = 10^3 is shown in figs. 4 and 5, respectively. As shown in these figures *via* existence of symmetrical geometry and boundary conditions relative to vertical midline of the cavity in the cases of top-top, middle-middle, and bottom-bottom, symmetrical fluid

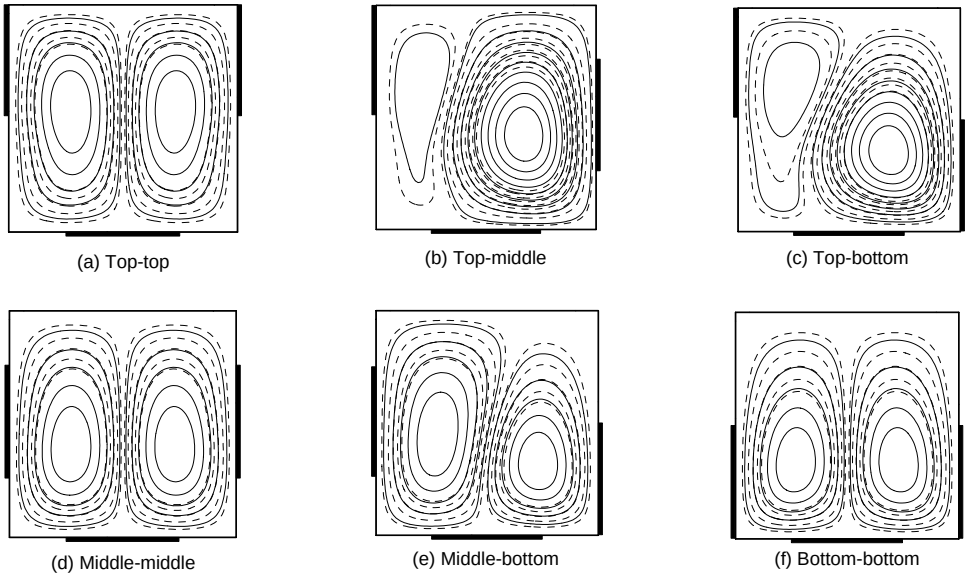

Figure 4. Streamlines for nanofluid with φ = 0.15 (solid lines) and pure water (dashed lines) for different arrangements of the heat sinks at Ra = 10^3

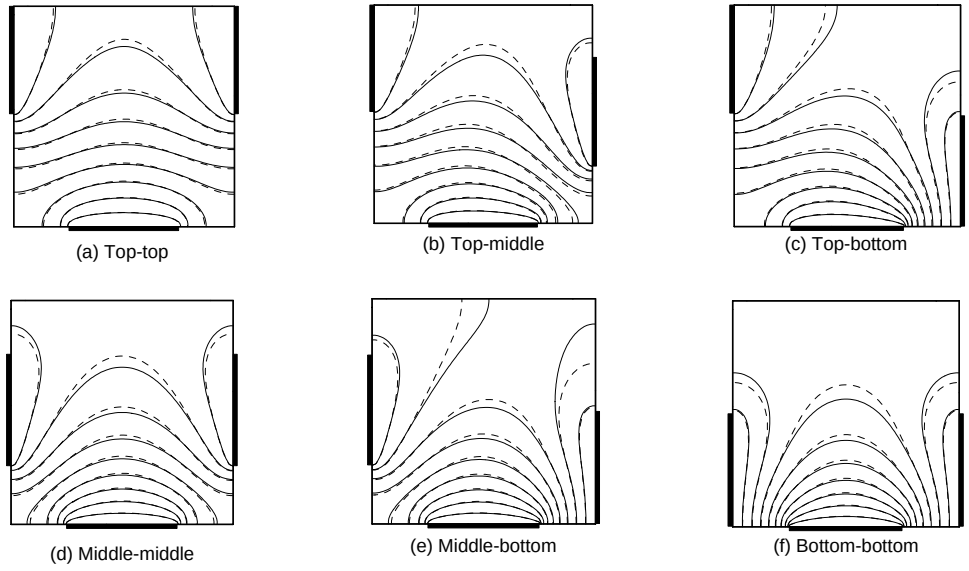

Figure 5. Isotherms for nanofluid with φ = 0.15 (solid lines) and pure water (dashed lines) for different arrangements of the heat sinks at Ra = 10^3

flow and temperature distribution are formed inside the cavity for these cases. For the mentioned symmetrical arrangements the heated fluid close to the heat source ascends, then cools and descends along the heat sink, hence two symmetrical counter rotating eddies are formed inside the cavity. For the bottom-bottom arrangement, the cores of these eddies are located in

lower half of the cavity. When the location of the symmetrical heat sinks moves upward, the cores of the vortexes move upward too. For the cases of top-middle, top-bottom, and middle-bottom, which non-symmetrical boundary conditions exist on the vertical walls, non-symmetrical flow and temperature fields are formed inside the cavity. For the top-middle case two counter rotating eddies are formed inside the cavity which the right eddy is greater and stronger than the left one. Similar observations are found in the top-bottom case with the difference of increasing the size of left eddy and decreasing the size of right eddy in comparison with those of the top-middle case. A different behavior is observed for the case of middle-bottom. In this case the left eddy is bigger than the right one. It can be observed from the isotherms in fig. 5 that a thermal stratification occurs in the lower region of the cavity. For the bottom-bottom case, the nanofluid existing in upper half of the cavity is isothermal. *Via* domination of conduction at Ra = 10^3, increase in the effective dynamic viscosity of the nanofluid *via* increase in the volume fraction of the nanoparticles does not affect the flow and temperature fields significantly in comparison with those of the pure fluid.

Streamlines and isotherms for six different considered arrangements of heat sinks for pure fluid and nanofluid with $\varphi = 0.15$ at Ra = 10^4 are shown in figs. 6 and 7, respectively. Similar to the results at Ra = 10^3, two symmetrical counter rotating eddies and symmetrical temperature distribution are observed inside the cavity for the top-top, middle-middle, and bottom-bottom arrangements.

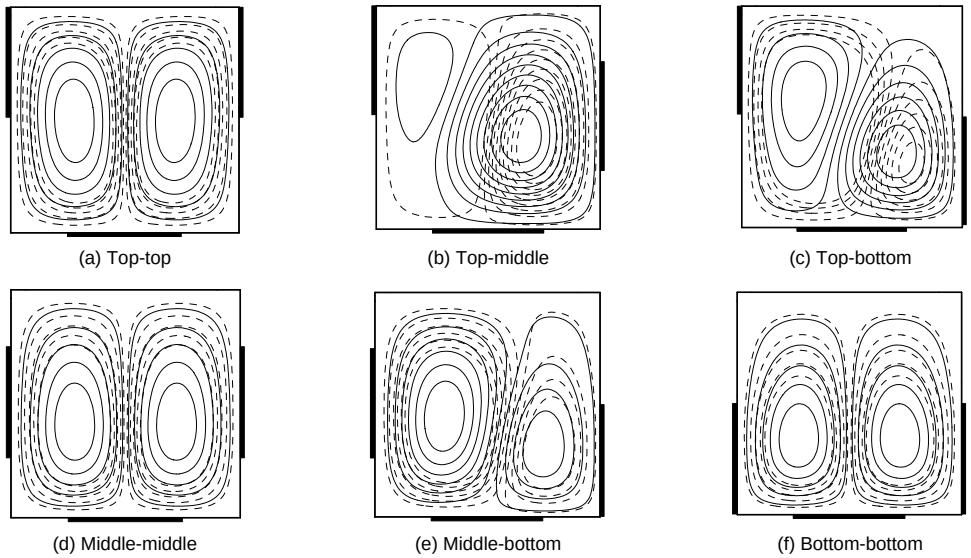

Figure 6. Streamlines for nanofluid with $\varphi = 0.15$ (solid lines) and pure water (dashed lines) for different arrangements of the heat sinks at Ra = 10^4

Differently from the results of Ra = 10^3, at Ra = 10^4 in the cases of top-middle, top-bottom, and middle-bottom, for the results of the pure fluid, the right eddy are smaller than the left one, while, a reverse behavior is found in top-middle and top-bottom arrangements for the results of the nanofluid. For non-symmetrical arrangements (top-middle, top-bottom, and middle-bottom) distance between the heat source and the right heat sink is shorter than the distance between the heat source and the left heat sink. Therefore the right eddy is stronger than the left eddy, hence increase in the effective dynamic viscosity of the nanofluid *via*

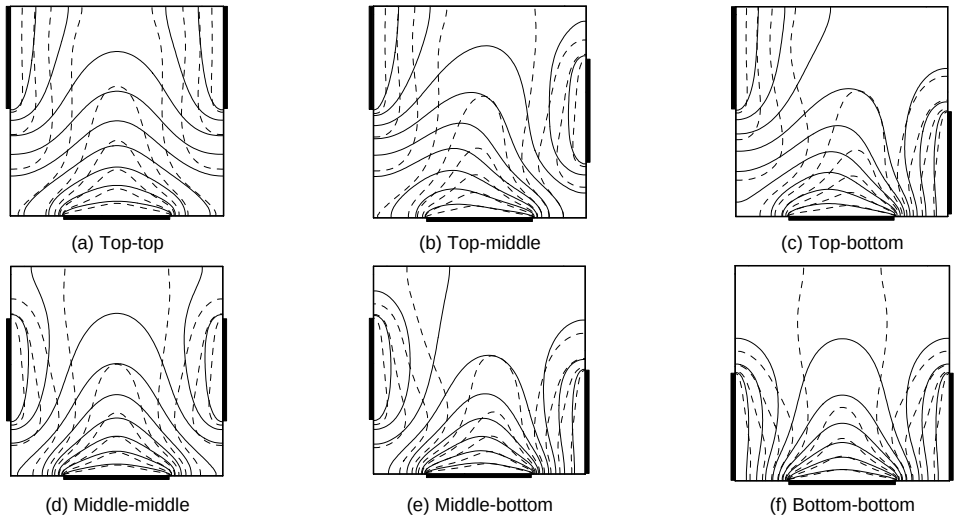

Figure 7. Isotherms for nanofluid with φ = 0.15 (solid lines) and pure water (dashed lines) for different arrangements of the heat sinks at Ra = 10^4

increase in the nanoparticles volume fraction motivates the right and left eddies to increases and decreases in size, respectively. When the volume fraction of the nanoparticles increases, thermal conductivity of the nanofluid increases which motivates increase in diffusion of heat inside the cavity. Temperature distribution of the nanofluid for all considered arrangements at Ra = 10^4 shows characteristics of conduction heat transfer while results of pure fluid show steeper temperature gradient adjacent to the isothermal wall which is characteristics of heat convection.

Streamlines and isotherms for nanofluid with φ = 0.15 and pure fluid at Ra = 10^5 for six different arrangements of heat sinks are shown in figs. 8 and 9, respectively. Similar to the

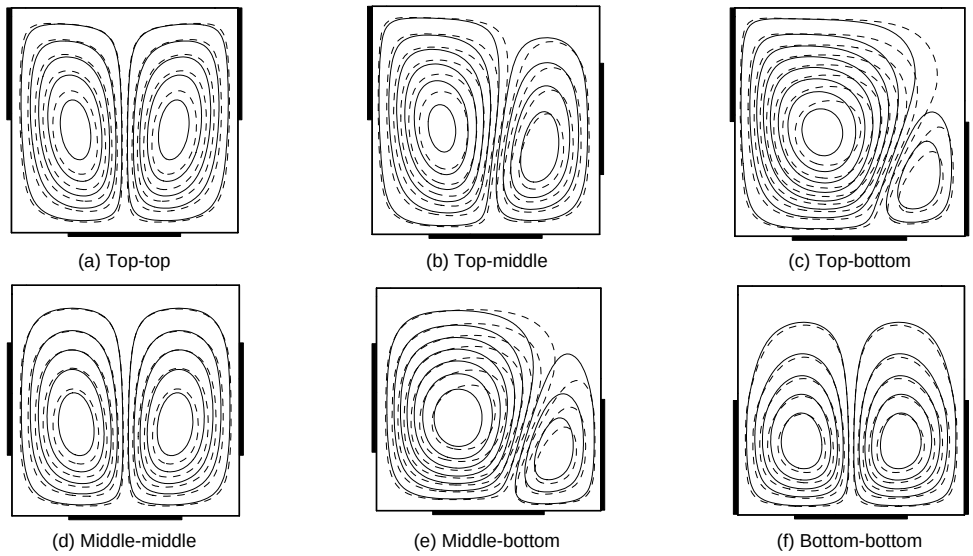

Figure 8. Streamlines for nanofluid with φ = 0.15 (solid lines) and pure water (dashed lines) for different arrangements of the heat sinks at Ra = 10^5

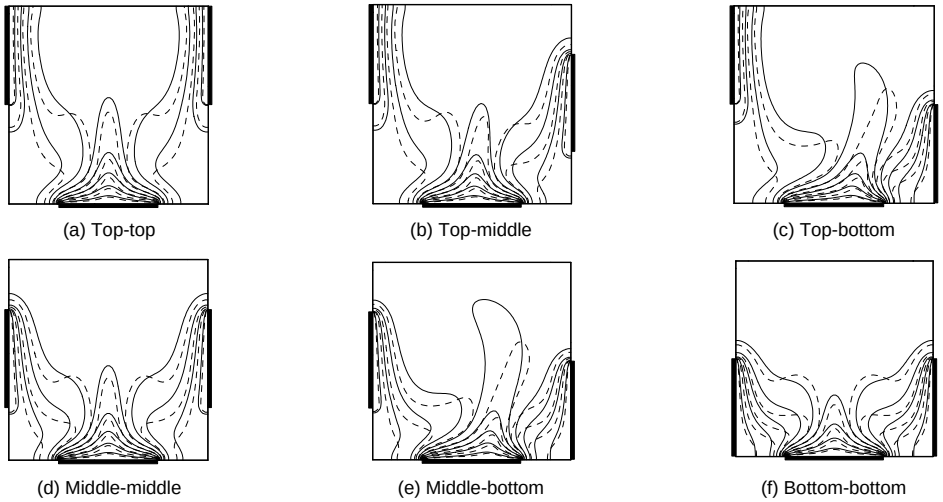

Figure 9. Isotherms for nanofluid with φ = 0.15 (solid lines) and pure water (dashed lines) for different arrangements of the heat sinks at Ra = 10^5

results at lower Rayleigh number, two symmetrical counter rotating eddies are formed inside the cavity for the top-top, middle-middle, and bottom-bottom arrangements. For the bottom-bottom case, the heat source and the heat sinks are located nearly and the cores of these eddies are located in lower half of the cavity. As the location of the heat sinks moves upward (the middle-middle and top-top cases) the location of the cores of these eddies moves upward too. For the top-middle, top-bottom, and middle-bottom arrangements, two non-symmetrical counter rotating eddies are formed inside the cavity which the right eddy is smaller than the left one. In these non-symmetrical cases, increasing the viscosity of the nanofluid *via* increasing the nanoparticles volume fraction motivates the left eddy, which is weaker than the right eddy, decreases in size. The isotherms in fig. 9 show that for bottom-bottom case the major upper portion of the cavity is isothermal. Moreover it is observable that the isotherms of pure fluid are more condensed in the vicinity of the side walls in comparison with those of the nanofluid.

Streamlines and isotherms of nanofluid with φ = 0.15 and pure fluid in all six arrangements at Ra = 10^6 are shown in figs. 10 and 11, respectively. In the top-top, middle-middle, and bottom-bottom cases, two symmetrical counter rotating eddies are observed inside the cavity. For the top-top and the middle-middle cases the cores of these eddies are elongated from down to the top of the cavity and are located in the middle region of the cavity while in bottom-bottom case the cores are located in lower half and near the vertical mid line of the cavity. Similar to the results of lower Rayleigh numbers, in non-symmetrical cases with increase in the volume fraction of the nanoparticles the right eddy, which is stronger than the left one, increases in size.

When the streamlines of each arrangement in figs. 4, 6, 8, and 10 are compared, the following results are obtained. In symmetrical cases (top-top, middle-middle, and bottom-bottom) when the Rayleigh number increases, no significant change occurs in flow pattern. In top-middle case, the size of the left eddy which is greater than the size of right eddy at Ra = 10^3, increases with increase in the Rayleigh number and finally at Ra = 10^6 a reverse behavior is observed. Increase in size of left eddy and decrease in size of right eddy by increase in the Rayleigh number can be observed in the cases of top-bottom and middle-bottom.

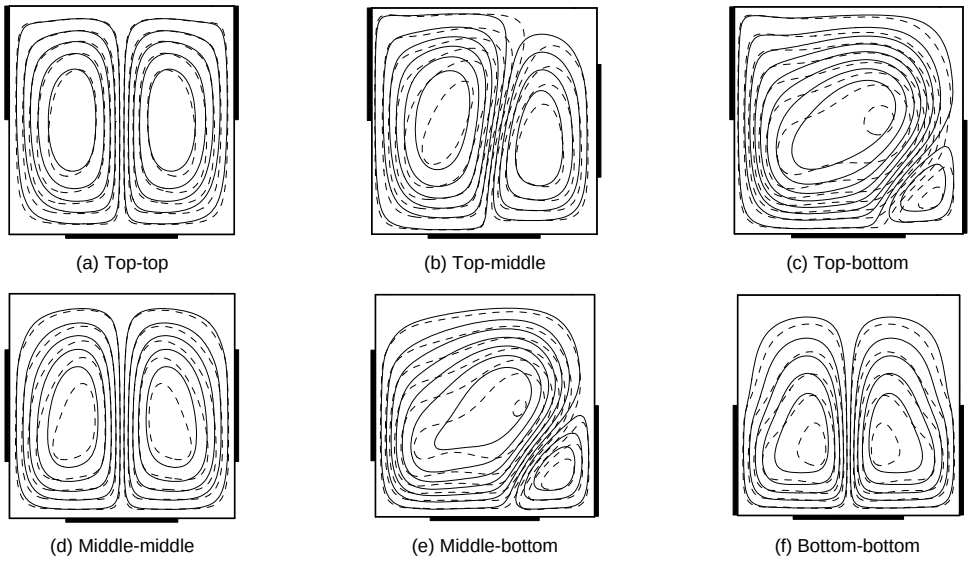

Figure 10. Streamlines for nanofluid with φ = 0.15 (solid lines) and pure water (dashed lines) for different arrangements of the heat sinks at Ra = 10^6

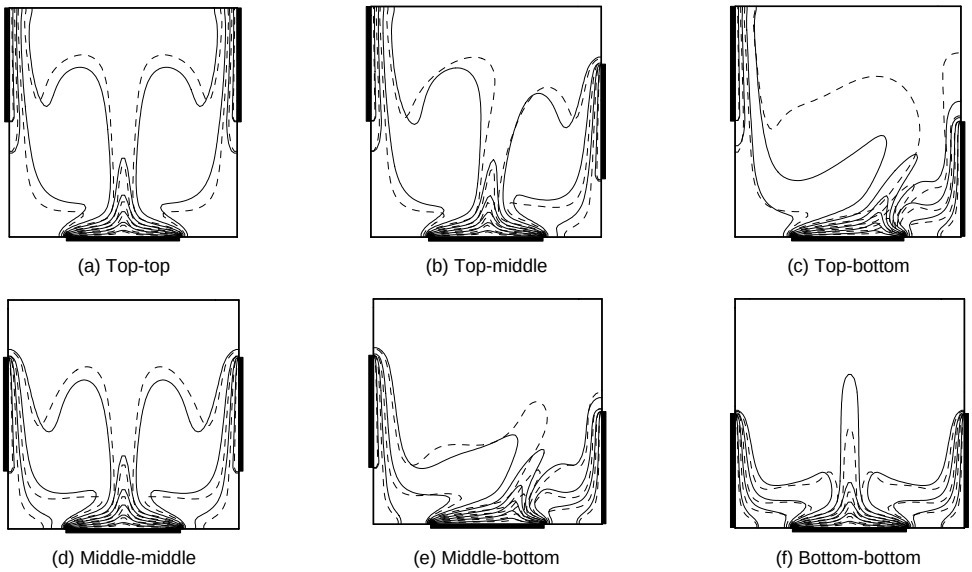

Figure 11. Isotherms for nanofluid with φ = 0.15 (solid lines) and pure water (dashed lines) for different arrangements of the heat sinks at Ra = 10^6

Variation of maximum absolute value of stream function with the volume fraction of the nanoparticles for all considered arrangements is shown in fig. 12 for each Rayleigh number separately. As shown in fig. 12(a), at Ra = 10^3 maximum absolute value of stream function occurs for top-top arrangement while its minimum occurs for top-middle arrangement. Results of the cases of top-middle and top-bottom coincide approximately. It can be observed

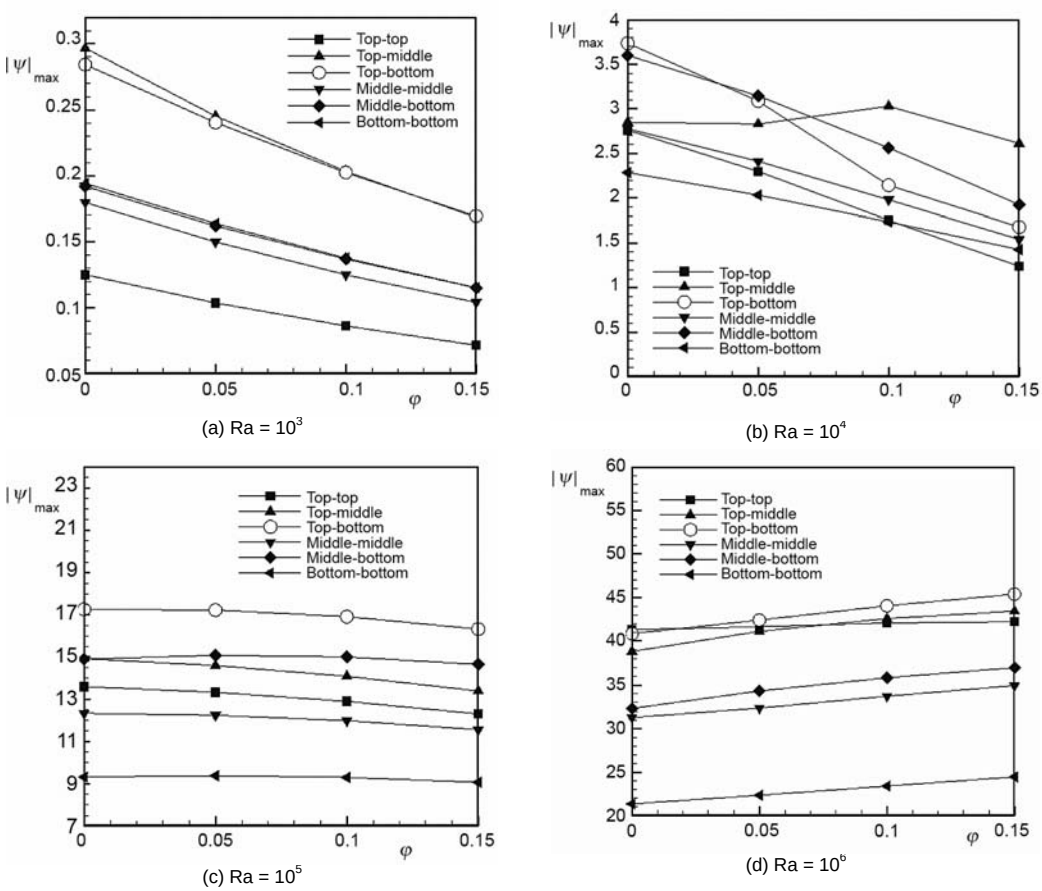

Figure 12. Maximum absolute value of streamfunction *vs.* nanoparticles volume fraction

that for all cases, the maximum absolute value of stream function is a decreasing function of the volume fraction of the nanoparticles. At Ra = 10^4, fig. 12(b), which conduction and convection are comparable, for top-middle cases with increase in the nanoparticles volume fraction the maximum absolute value of stream function initially increases and then decreases. For all other cases the maximum absolute value of stream function is a decreasing function of the nanoparticles volume fraction. For this Rayleigh number, the bottom-bottom case has minimum flow strength while the top-middle and middle-bottom cases have maximum flow strength. At high Rayleigh numbers (Ra = 10^5 and 10^6) the heat transfer occurs mainly through convection. As shown in figs. 12(c) and (d), the top-bottom case has maximum flow strength. This is because of short distance between the heat source and right heat sink compared to the other cases. At these Rayleigh numbers minimum flow strength occurs for bottom-bottom case.

Variation of the average Nusselt number of the heat source with the nanoparticles volume fraction for each Rayleigh number is shown in fig. 13. As shown in fig. 13(a), at Ra = 10^3 for all cases the average Nusselt number increases with a same rate by increase in the volume fraction of the nanoparticles. At Ra = 10^3 heat transfer occurs mainly through conduction and minimum distance between the heat source and sinks in the bottom-bottom case, motivate highest rate of heat transfer for this case. With increase in the distance between

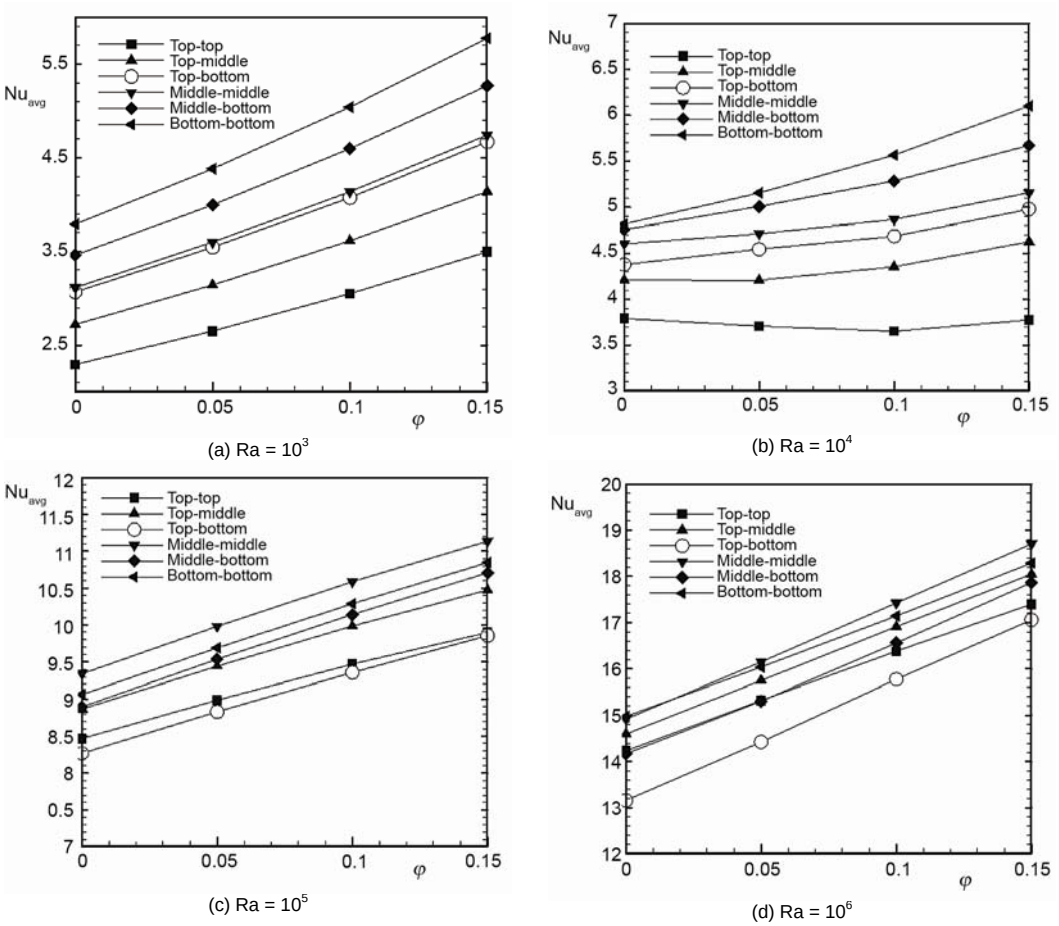

Figure 13. Average Nusselt number of the heat source *vs.* nanoparticles volume fraction

the source and sinks, the average Nusselt number decreases and finally minimum rate of heat transfer occurs in top-top case with the largest distance between the heat source and sinks. As shown in fig. 13(b) at Ra = 10^4, for different heat sinks arrangements with increase in the volume fraction of the nanoparticles, different trends are found. It is observed from the figure that as the average Nusselt number decreases by change in the configurations of the heat sinks, the rate of increase in the average Nusselt number with increase in the nanofluid volume fraction decreases too. At this Rayleigh number, which conduction and convection are comparable, the maximum rate of heat transfer occurs for the bottom-bottom case. With increase in the distance between heat source and sinks, the average Nusselt number and the rate of increase in the average Nusselt number with increase in the nanoparticles volume fraction, decreases and finally a decreasing trend in the average Nusselt number with the nanoparticles volume fraction is found for the top-top arrangements. Average Nusselt number at Ra = 10^5 and 10^6 are shown in figs. 13(c) and (d), respectively. At these Rayleigh numbers heat transfer occurs mainly through convection. Differently from results of Ra = 10^3 and 10^4, maximum rate of heat transfer occurs for the middle-middle case. A relatively lower heat transfer occurs for the bottom-bottom case. *Via* blockage effect of the top wall the top-top case has a low heat transfer rate. Lowest average Nusselt number occurs for top-bottom.

To make a comparison between effects of different water based nanofluid in enhancement of heat transfer, the middle-middle case is chosen and five different nanofluids, namely, Cu-water, Ag-water, Al_2O_3-water, CuO-water, and TiO_2-water are employed. Figure 14 shows variation of the average Nusselt number of the heat source with the nanoparticles volume fraction in the middle-middle arrangement for different considered nanofluids at each Rayleigh numbers separately. Figure 14(a) shows results of Ra = 10^3. As can be seen from the figure at this Rayleigh number, which conduction dominates the heat transfer, maximum rate of heat transfer occurs for Ag-Water nanofluid with the highest thermal conductivity and its minimum rate occurs for TiO_2-water nanofluid with the lowest thermal conductivity. Moreover it is observable that for each nanofluid the rate of increase in the average Nusselt number with increase in the volume fraction of the nanoparticles doesn't change with change in the volume fraction of the nanoparticles approximately. As can be seen from fig. 14(b), at Ra = 10^4 maximum rate of heat transfer occurs for Cu-water nanofluid and its minimum occurs for TiO_2-water nanofluid. Also at this Rayleigh number the rate of increase in the average Nusselt number with increase in the nanoparticles volume fraction, increases by increase in the nanoparticles volume fraction. At Ra = 10^5 and 10^6, maximum and minimum rate of heat transfer occurs for Cu-water and

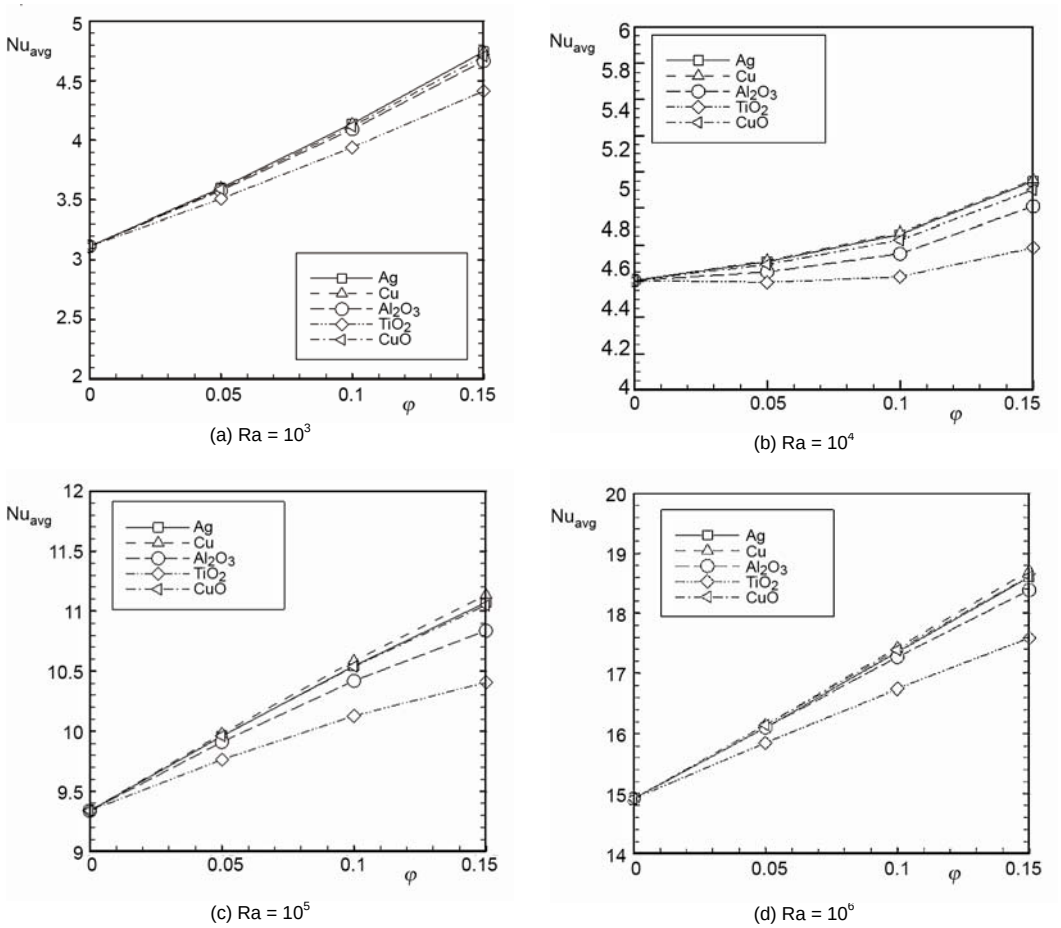

Figure 14. Average Nusselt number of the heat source *vs.* nanoparticles volume fraction for different water based nanofluids

TiO_2-water nanofluid, respectively. Moreover at these Rayleigh numbers, rate of increase in the average Nusselt number decreases by increase in the nanoparticles volume fraction.

Conclusions

The problem of free convection of Cu-water nanofluid inside a square cavity with a heat source on its bottom wall and two heat sinks with six different location on its side walls has been investigated numerically using the finite volume method and SIMPLER algorithm. A parametric study was undertaken and effects of the Rayleigh number, the volume fraction of the nanoparticles, and arrangements of the heat sinks were investigated. Also for the middle–middle arrangement, the capability of five different water based nanofluids has been examined. The obtained results show that the average Nusselt number of the heat source increases with increase in the Rayleigh number and the volume fraction of the nanoparticles. Moreover it is found that at low Rayleigh numbers (conduction dominant regime) maximum and minimum rate of heat transfer occur for the bottom-bottom and top-top arrangements, respectively, while; at high Rayleigh numbers (convection dominant regime) its maximum and minimum occur for the middle-middle and top-bottom cases, respectively. Results of different nanofluid for the middle-middle case show that at low Rayleigh number, maximum and minimum rate of heat transfer are obtained by Ag-water and TiO_2-water nanofluids, while; at high Rayleigh numbers its maximum and minimum are obtained by Cu-water and TiO_2-water nanofluids.

Nomenclature

Cp – specific heat, [$Jkg^{-1}K^{-1}$]
g – gravitational acceleration, [ms^{-2}]
H – enclosure height, [m]
h – heat transfer coefficient, [$Wm^{-2}K^{-1}$]
k – thermal conductivity, [$Wm^{-1}K^{-1}$]
Nu – Nusselt number, [–]
p – pressure, [Nm^{-2}]
P – dimensionless pressure, [–]
Pr – Prandtl number, [–]
q – heat flux, [Wm^{-2}]
Ra – Rayleigh number, [–]
T – dimensional temperature, [K]
u, v – dimensional velocities components in x- and y-direction, [$m\ s^{-1}$]
U, V – dimensionless velocities components in x- and y-direction, [–]
x, y – dimensional Cartesian coordinates, [m]
X, Y – dimensionless Cartesian coordinates, [–]

Greek symbols

α – thermal diffusivity, [m^2s]
β – thermal expansion coefficient, [K^{-1}]
θ – dimensionless temperature, [–]
μ – dynamic viscosity, [$kgm^{-1}s^{-1}$]
ν – kinematic viscosity, [m^2s^{-1}]
ρ – density, [kgm^{-3}]
φ – volume fraction of the nanoparticles, [–]
ψ – stream function, [m^2s^{-1}]

Subscripts

c – cold
f – fluid
h – hot
nf – nanofluid
s – solid particles
w – wall

References

[1] Ostrach, S., Natural Convection in Enclosures, *ASME J. Heat Transfer, 110 (4b)* (1988) pp. 1175-1190
[2] Choi, U. S., Enhancing Thermal Conductivity of Fluids with Nanoparticles, *ASME FED, 231* (1995), pp. 99-105
[3] Kang, H. U., *et al.*, Estimation of Thermal Conductivity of Nanofluid Using Experimental Effective Particle Volume, *Exp. Heat Transfer, 19* (2006), 3, pp. 181-191
[4] Velagapudi, V., *et al.*, Empirical Correlation to Predict Thermophysical and Heat Transfer Characteristics of Nanofluids, *Thermal Science, 12* (2008), 1, pp. 27-37
[5] Turgut, A., *et al.*, Thermal Conductivity and Viscosity Measurements of Water-Based TiO_2 Nanofluids, *Int. J. Thermophys, 30 (4)* (2009), pp. 1213-1226
[6] Rudyak, V. Y., *et al.*, On the Thermal Conductivity of Nanofluids, *Technical Physics Letters, 36 (7)* (2010), pp. 660-662

[7] Murugesan, C., Sivan, S., Limits for Thermal Conductivity of Nanofluids, *Thermal Science, 14 (1)* (2010), 1, pp. 65-71
[8] Nayak, A. K., *et al.*, Measurement of Volumetric Thermal Expansion Coefficient of Various Nanofluids, *Technical Physics Letters, 36 (8)* (2010), pp. 696-698
[9] Khanafer, K., *et al.*, Buoyancy-Driven Heat Transfer Enhancement in a Two-Dimensional Enclosure Utilizing Nanofluid, *Int. J. Heat Mass Tran., 46 (19)* (2003), pp. 3639-3653
[10] Santra, A. K., *et al.*, Study of Heat Transfer Augmentation in a Differentially Heated Square Cavity Using Copper-Water Nanofluid, *Int. J. Thermal Sci., 47 (9)* (2008), pp. 1113-1122
[11] Oztop, H. F., Abu-Nada, E., Numerical Study of Natural Convection in Partially Heated Rectangular Enclosures Filled with Nanofluids, *Int. J. Heat Fluid Flow, 29 (5)* (2008), pp. 1326-1336
[12] Abu-nada, E., Oztop, H., Effect of Inclination Angle on Natural Convection in Enclosures Filled with Cu-Water Nanofluid, *Int. J. Heat Fluid Flow, 30 (4)* (2009), pp. 669-678
[13] Aminossadati, S. M., Ghasemi, B., Natural Convection Cooling of a Localized Heat Source at the Bottom of a Nanofluid-Filled Enclosure, *European Journal of Mechanic B/Fluids, 28 (5)* (2009), pp. 630-640
[14] Ghasemi, B., Aminossadati, S. M., Periodic Natural Convection in a Nanofluid-Filled Enclosure with Oscillating Heat Flux, *Int. J. Thermal Sci., 49 (1)* (2010), pp. 1-9
[15] Saleh, H., *et al.*, Natural Convection Heat Transfer in a Nanofluid-Filled Trapezoidal Enclosure, *Int. J. Heat Mass Transfer 54 (1-3)* (2011), pp. 194-201
[16] Sheikhzadeh, G. A., *et al.*, Numerical Study of Natural Convection in a Differentially-Heated Rectangular Cavity Filled with TiO_2-Water Nanofluid, *Journal of Nano Research, 13* (2011), February, pp. 75-80
[17] Oztop, H. F., *et al.*, Computational Analysis of Non-Isothermal Temperature Distribution on Natural Convection in Nanofluid Filled Enclosures, *Superlattices and Microstructures, 49 (4)* (2011), 4, pp. 453-467
[18] Abbasian Arani, A. A., *et al.*, Free Convection in a Nanofluid Filled Square Cavity with an Horizontal Heated Plate, *Defect Diffusion Forum, 312-315* (2011), April, pp. 433-438
[19] Mahmoodi, M., Numerical Simulation of Free Convection of Nanofluid in a Square Cavity with an Inside Heater, *Int. J. Thermal Sci., 50 (11)* (2011), pp. 2161-2175
[20] Mahmoodi, M., Numerical Simulation of Free Convection of a Nanofluid in L-Shaped Cavities, *Int. J. Thermal Sci., 50 (9)* (2011), pp. 1731-1740
[21] Sourtiji, E., Hosseinizadeh, S. F., Heat Transfer Augmentation of Magnetohydrodynamic Natural Convection in L-Shaped Cavities Utilizing Nanofluids, *Thermal Science, 16* (2012), 2, pp. 489-501
[22] Nithyadevi, N., *et al.*, Natural Convection in a Rectangular Cavity with Partially Active Side Walls, *Int. J. Heat Mass Tran., 50 (23-24)* (2007), pp. 4688-4697
[23] Deng, Q. H., Fluid Flow and Heat Transfer Characteristics of Natural Convection in Square Cavities due to Discrete Source-Sink Pairs, *Int. J. Heat Mass Tran., 51 (25-26)* (2008), pp. 5949-5957
[24] Sheikhzadeh, G. A., *et al.*, Natural Convection of Cu-Water Nanofluid in a Cavity with Partially Active Side Walls, *European Journal of Mechanics B/Fluids, 30 (2)* (2011), pp. 166-176
[25] Bejan, A., *Convection Heat Transfer*, John Wiley & Sons, Inc., Hoboken, N. J., USA, 2004
[26] Brinkman, H. C., The Viscosity of Concentrated Suspensions and Solutions, *J. Chem. Phys., 20* (1952), pp. 571-581
[27] Maxwell, J., *A Treatise on Electricity and Magnetism*, 2nd ed., Oxford University Press, Cambridge, UK, 1904
[28] Patankar, S. V., *Numerical Heat Transfer and Fluid Flow,* Hemisphere Pub. Co., Washington., DC, 1980
[29] Hoffman, J. D., *Numerical Methods for Engineers and Scientists,* 2nd ed., Markel Dekker Inc., New York, USA, 2001
[30] Barakos, G., Mitsoulis, E., Natural Convection Flow in a Square Cavity Revisited: Laminar and Turbulent Models with Wall Fraction, *Int. J. Numer. Methods Fluids 18 (7)* (1994), pp. 695-719
[31] Davis, G. V., Natural Convection of Air in a Square Cavity, a Benchmark Numerical Solution, *Int. J. Numer. Methods Fluids, 3 (3)* (1983), pp. 249-264
[32] Fusegi, T., *et al.*, A Numerical Study of Tree-Dimensional Natural Convection in a Differentially Heated Cubical Enclosure, *Int. J. Heat Mass Tran., 34* (1991), 6, pp. 1543-1557

Paper submitted: April 6, 2011
Paper revised: December 5, 2012
Paper accepted: January 30, 2013